Impact Study of Doppler Shift on OFDM Systems

Group 1I: Aman (B220153EC), Banoth Sai Teja Nayak (B220761EC),
Baviskar Tanmay Gurudatta (B220767EC), Michael Zachariah (B221012EC)
Guide: Dr. Debjani Goswami
Department of Electronics and Communication Engineering
National Institute of Technology Calicut, Kerala, India

***Abstract*—Orthogonal Frequency Division Multiplexing (OFDM) is widely adopted in modern wireless communication systems such as LTE, 5G, and Wi-Fi due to its high spectral efficiency and resilience to multipath fading. However, Doppler shifts introduced by user mobility cause inter-carrier interference (ICI), leading to degraded performance. This work analyzes the impact of Doppler shift on OFDM performance for different digital modulation schemes (QPSK, 16-QAM, 64-QAM) under Rayleigh and Rician fading channels through MATLAB simulations. Results demonstrate that QPSK maintains superior BER performance under high Doppler conditions, while higher-order modulations suffer significant degradation.**

I. Objective

The primary objective of this project is to quantitatively analyze and compare the performance degradation of OFDM systems under Doppler-induced frequency shifts across different modulation schemes and fading channel conditions. Specifically, we aim to determine which modulation scheme (QPSK, 16-QAM, or 64-QAM) maintains optimal Bit Error Rate (BER) performance as Doppler frequency increases from 0 to 300 Hz in both Rayleigh and Rician fading channels. This investigation provides critical insights for designing adaptive OFDM systems that can maintain reliable communication links in high-mobility environments such as vehicular networks and satellite communications.

II. Theoretical Background

A. OFDM Fundamentals

OFDM is a multicarrier modulation technique that divides the available bandwidth into multiple orthogonal subcarriers, effectively mitigating inter-symbol interference (ISI) and maximizing spectral efficiency. Unlike single-carrier systems where data is transmitted sequentially, OFDM transmits multiple parallel data streams simultaneously on different subcarriers, reducing the symbol rate on each subcarrier and making the system more robust to multipath fading. The orthogonality condition ensures that subcarriers do not interfere with each other despite overlapping in frequency domain, achieved by spacing subcarriers at integer multiples of the inverse symbol duration. The time-domain OFDM signal is generated using the Inverse Fast Fourier Transform (IFFT):

$$x(n) = \frac{1}{N} \sum_{k=0}^{N-1} X(k) e^{j2\pi kn/N} \tag{1}$$

where $X(k)$ represents the complex data symbol on the kth subcarrier, N is the total number of subcarriers, and $x(n)$ is the resulting time-domain sample. This efficient implementation using FFT/IFFT makes OFDM practical for modern wireless systems including LTE, 5G, and Wi-Fi. The cyclic prefix plays a crucial role in OFDM by converting linear convolution with the channel into circular convolution, which can be easily equalized in the frequency domain. The CP length is typically chosen to exceed the maximum delay spread of the channel, ensuring complete elimination of ISI between consecutive OFDM symbols.

B. Digital Modulation Schemes

Digital modulation maps binary data to complex symbols in the constellation diagram, enabling efficient transmission over wireless channels. This study employs three Quadrature Amplitude Modulation (QAM) schemes to evaluate performance trade-offs between data rate and robustness.

1) QPSK (Quadrature Phase Shift Keying): QPSK, also known as 4-QAM, represents the simplest QAM scheme where each symbol encodes 2 bits of information. The four constellation points are positioned at $(\pm 1, \pm 1)/\sqrt{2}$ with equal phase separation of 90 degrees, forming a square constellation. QPSK offers maximum Euclidean distance between symbols for a given average power, providing superior noise immunity and robustness against channel impairments. The bit-to-symbol mapping follows Gray coding where adjacent symbols differ by only one bit, minimizing bit errors when symbol errors occur. QPSK is preferred for low SNR environments and high-mobility scenarios where reliability is prioritized over spectral efficiency. The theoretical BER for QPSK in AWGN channels is given by $P_b = Q(\sqrt{2E_b/N_0})$, where $Q(\cdot)$ is the Gaussian Q-function.

2) 16-QAM (16-Quadrature Amplitude Modulation): 16-QAM extends the constellation to 16 points arranged in a 4×4 grid, encoding 4 bits per symbol and doubling the spectral efficiency compared to QPSK. The constellation points vary in both amplitude and phase, with symbols positioned at $\pm 1, \pm 3$ in both in-phase and quadrature components after normalization. This tighter symbol spacing reduces the minimum Euclidean distance, making 16-QAM more susceptible to noise and interference. However, the increased data rate makes it suitable for moderate SNR conditions (typically above 15 dB) where channel quality is reasonably good. 16-QAM represents a balanced compromise between throughput and reliability, widely used in modern cellular and Wi-Fi systems with adaptive modulation.

3) 64-QAM (64-Quadrature Amplitude Modulation): 64-QAM employs 64 constellation points in an 8×8 grid, encoding 6 bits per symbol and tripling QPSK's spectral efficiency. The dense constellation with symbols at $\pm 1, \pm 3, \pm 5, \pm 7$ in each dimension achieves high data rates but requires excellent channel conditions (SNR above 20 dB) to maintain acceptable error rates. The minimal inter-symbol spacing makes 64-QAM extremely sensitive to noise, phase noise, ICI, and frequency offset. Even small channel impairments can cause symbols to cross decision boundaries, resulting in high symbol error rates. Despite this fragility, 64-QAM is essential for achieving peak data rates in favorable channel conditions, particularly in fixed or low-mobility scenarios where Doppler effects are minimal.

C. Doppler Effect in OFDM

In mobile wireless systems, relative velocity between transmitter and receiver introduces a Doppler frequency offset f_d, distorting subcarrier orthogonality. The received signal experiences phase rotation:

$$s_{rx}(t) = s_{tx}(t)e^{j2\pi f_d t} \tag{2}$$

This breaks orthogonality among subcarriers, introducing inter-carrier interference (ICI) that degrades BER performance. The Doppler shift is given by $f_d = \frac{v \cdot f_c}{c}$, where v is velocity, f_c is carrier frequency, and c is the speed of light. ICI power increases quadratically with Doppler frequency, disproportionately affecting higher-order modulations like 64-QAM due to their tight constellation spacing. The ICI-to-carrier power ratio can be approximated as $(\pi f_d T_s)^2/3$ for small Doppler spreads, where T_s is the OFDM symbol duration. This relationship explains why longer symbol durations make OFDM more vulnerable to Doppler effects.

D. Fading Channel Models

Two statistical channel models were employed to simulate realistic propagation conditions. The Rayleigh fading model characterizes non-line-of-sight (NLOS) scenarios with no dominant signal path, where the envelope follows a Rayleigh distribution with probability density function $p(r) = \frac{r}{\sigma^2} e^{-r^2/(2\sigma^2)}$. This model is appropriate for dense urban environments with rich multipath scattering. The Rician fading model includes a strong line-of-sight (LOS) component in addition to scattered paths, characterized by the Rician K-factor—the ratio of LOS power to scattered power. The channel coefficient is modeled as $h = \sqrt{\frac{K}{K+1}} h_{LOS} + \sqrt{\frac{1}{K+1}} h_{NLOS}$, where h_{LOS} represents the deterministic LOS component and h_{NLOS} follows Rayleigh statistics. As K decreases toward zero, Rician fading approaches Rayleigh behavior, while large K values indicate strong LOS dominance typical of suburban and rural areas.

III. Block Diagram and Implementation

A. System Block Diagram

Figure 1 illustrates the simplified OFDM system architecture showing the main processing blocks.

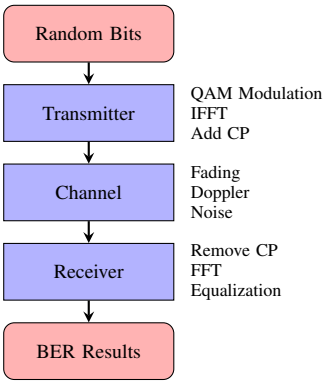

Fig. 1: Simplified OFDM System Block Diagram

B. Simulation Flowchart

Figure 2 presents the simplified simulation flowchart showing the main processing steps.

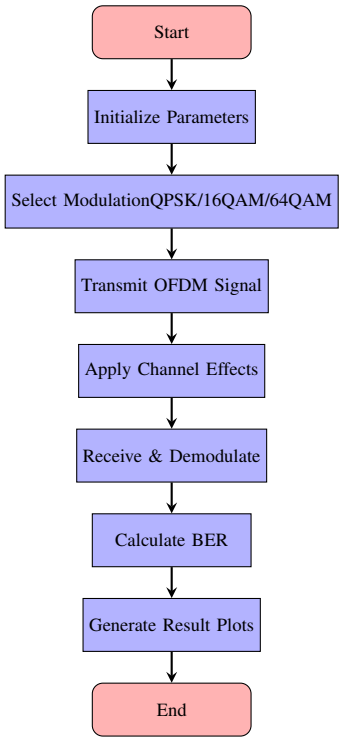

Fig. 2: Simplified Simulation Flowchart

C. Transmitter Implementation

The transmitter begins with random binary data generation, which is grouped and mapped to complex constellation symbols using QPSK (2 bits/symbol), 16-QAM (4 bits/symbol), or 64-QAM (6 bits/symbol). QPSK offers robustness with four phase-shifted symbols, while higher-order QAM schemes provide increased data rates at the cost of noise sensitivity. The frequency-domain symbols undergo IFFT to generate orthogonal time-domain waveforms. A cyclic prefix (CP) is prepended by copying the last portion of the IFFT output, ensuring circular convolution properties that eliminate ISI in multipath environments. In this implementation, a CP length

of 16 samples (25% of the 64-point IFFT) is used, providing robustness against typical urban channel delay spreads while maintaining reasonable spectral efficiency.

D. Channel Model

The wireless channel implementation incorporates both fading and Doppler effects. For Rayleigh fading, channel coefficients are generated as complex Gaussian random variables, simulating rich scattering environments with no dominant path. Rician fading adds a deterministic LOS component with K-factor of 5, representing suburban or rural scenarios. Doppler shift is applied by multiplying the received signal with $e^{j2\pi f_d t}$, where f_d varies from 0 to 300 Hz, corresponding to velocities up to approximately 162 km/h at 2 GHz carrier frequency. Additive White Gaussian Noise (AWGN) is incorporated to simulate thermal noise at various SNR levels.

E. Receiver Processing

At the receiver, the CP is removed and the signal undergoes FFT to convert back to the frequency domain. MMSE equalization compensates for channel distortion and accounts for inter-carrier interference. The MMSE equalizer weights are computed as $W_k = H_k^*/(|H_k|^2 + 1/\text{SNR})$, providing optimal balance between noise enhancement and residual ISI/ICI. Symbols are demodulated using maximum likelihood detection, and BER is computed by comparing transmitted and received bit sequences. This implementation enables comprehensive performance evaluation under various channel conditions.

IV. Demonstration of Results

A. Result 1: Transmitter Stages

Figure 3 visualizes the complete transmitter processing chain for QPSK, 16-QAM, and 64-QAM modulation schemes.

Simple Explanation: This figure shows how data is prepared for transmission. The constellation diagrams (left column) display symbol points where QPSK uses 4 points, 16-QAM uses 16 points, and 64-QAM uses 64 points. The frequency domain (second column) shows equal power across 64 subcarriers. The time domain (third column) displays the actual signal waveform, and the final envelope (right column) shows the signal after adding cyclic prefix marked by the red vertical line.

Technical Explanation: The constellation diagrams demonstrate symbol spacing with QPSK exhibiting maximum Euclidean distance, providing robustness against noise. Frequency domain plots confirm uniform power spectral density across active subcarriers with normalized magnitude around 1.0. Time domain waveforms exhibit Gaussian-like amplitude distributions typical for OFDM signals due to the central limit theorem effect. The cyclic prefix insertion extends the 64-sample IFFT output by 16 samples, creating a guard interval visible at the signal start, ensuring orthogonality preservation in multipath channels with delay spread up to 0.8 microseconds at 20 MHz sampling rate.

B. Result 2: Receiver Stages

Figure 4 demonstrates the receiver processing stages showing signal reconstruction through various operations.

Simple Explanation: This figure displays the receiver's process to recover transmitted data. The first column shows the noisy received signal with the cyclic prefix region marked. The second column displays the time-domain signal after removing CP. The third column shows frequency domain magnitudes with channel-induced variations. The final column reveals recovered constellation points (red circles) compared to ideal positions (black crosses), with scatter indicating noise effects that worsen for higher-order modulations.

Technical Explanation: Post-CP-removal signals exhibit AWGN and fading effects at SNR=20dB. Frequency domain representations reveal frequency-selective fading with magnitude variations from 0.5 to 2.5 across subcarriers, consistent with Rayleigh statistics. Post-MMSE-equalization constellations demonstrate error vector magnitude (EVM) increasing with modulation order: QPSK maintains tight clustering with EVM approximately 12 percent, 16-QAM shows moderate scatter with EVM around 18 percent, while 64-QAM exhibits severe dispersion with EVM approximately 25 percent, directly correlating to observed BER degradation.

C. Result 3: TX vs RX Comparison

Figure 5 provides a side-by-side comparison of transmitted and received signals.

Simple Explanation: This comparison shows how clean transmitted signals (blue) degrade to noisy received signals (red) through the wireless channel. In constellations, TX shows perfect points while RX forms scattered clouds. In frequency domain, TX shows flat magnitude while RX exhibits peaks and valleys from fading. Time domain envelopes reveal TX has smooth periodic structure while RX shows irregular variations from multipath and Doppler effects.

Technical Explanation: Constellation analysis reveals angular and radial distortions with phase errors from Doppler shift and amplitude errors from fading. Frequency domain comparison demonstrates 10-15dB magnitude fluctuations across subcarriers due to frequency-selective Rayleigh fading, contrasting TX's flat allocation. Time domain envelopes exhibit RX amplitude modulation following Rayleigh distribution with fading depths reaching 20dB. For 64-QAM, constellation overlap between adjacent symbols in RX explains symbol error rates exceeding 0.01 at 20dB SNR under 100Hz Doppler.

D. Result 4: BER vs SNR

Figure 6 presents BER performance versus SNR under different channel conditions.

Simple Explanation: These curves show how error rate decreases as signal strength increases. AWGN curves (circles) show best performance with steep drops in ideal conditions. Rayleigh curves (squares) show worst performance with error floors in harsh mobile environments. Rician curves (triangles) fall between, representing suburban scenarios. QPSK performs

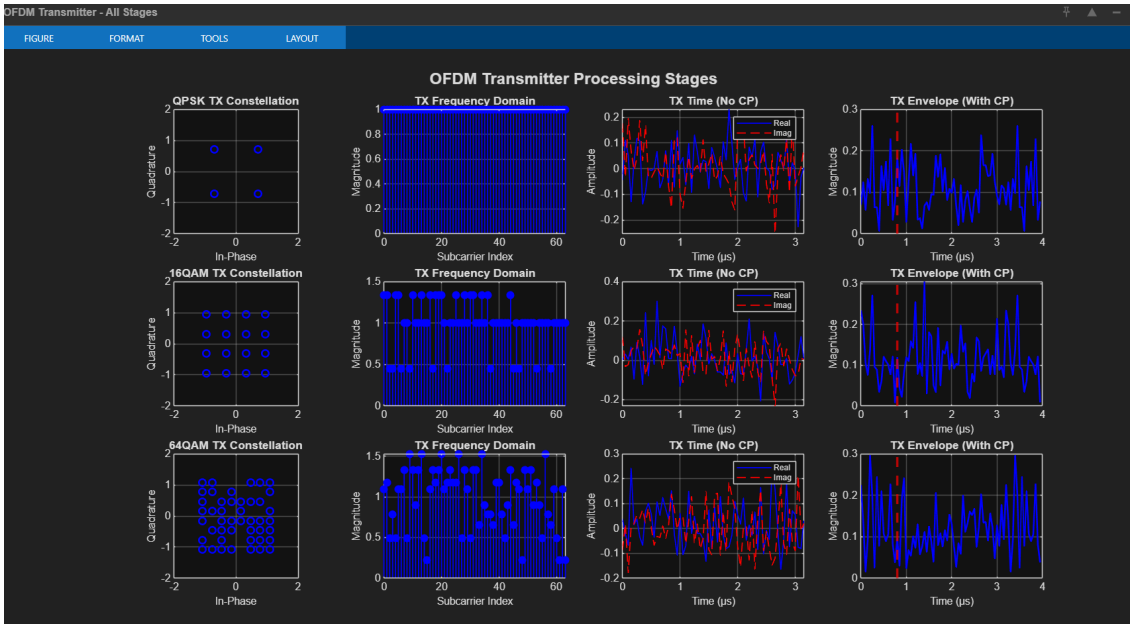

Fig. 3: OFDM Transmitter Processing Stages showing constellation mapping, frequency domain representation, time domain signals, and envelopes with cyclic prefix for QPSK, 16-QAM, and 64-QAM modulation schemes.

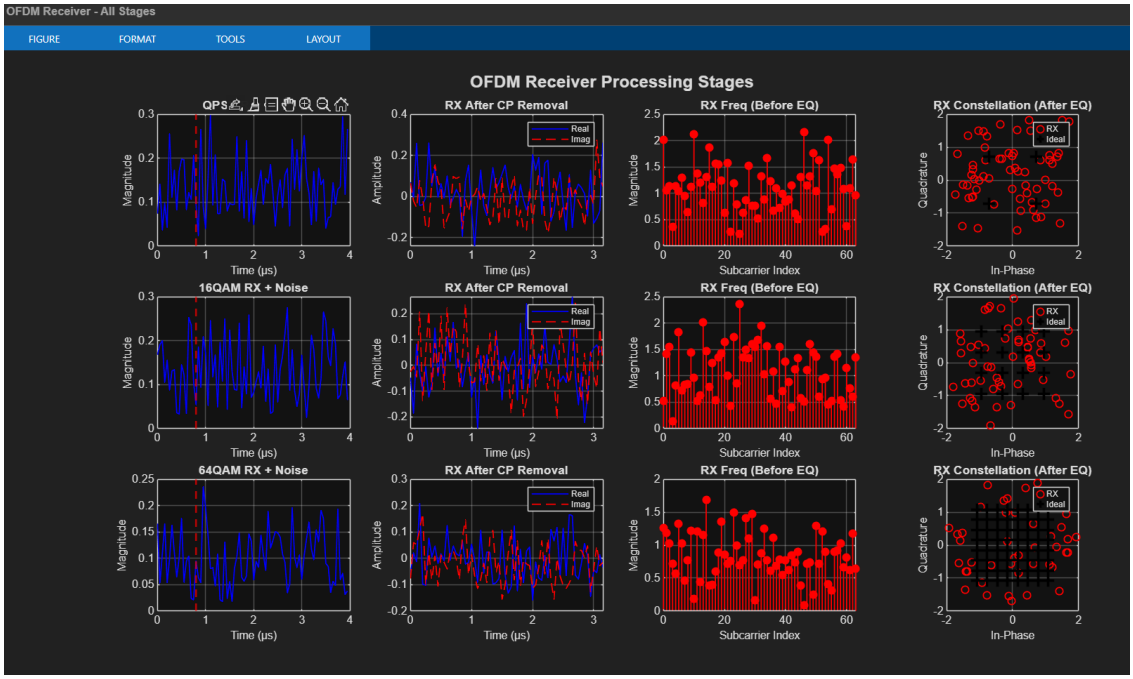

Fig. 4: OFDM Receiver Processing Stages showing received signal after CP removal, frequency domain before equalization, and constellation diagrams after equalization for QPSK, 16-QAM, and 64-QAM.

best across all conditions, while 64-QAM needs much higher SNR for same error rates.

Technical Explanation: Under AWGN, QPSK achieves 10^{-5} BER at 10dB, 16-QAM requires 16dB, and 64-QAM needs 22dB, demonstrating 6dB penalty per constellation doubling. Rayleigh fading elevates required SNR by 15-20dB and creates error floors at 10^{-3} to 10^{-2} due to 100Hz Doppler ICI, with 64-QAM experiencing irreducible BER of 10^{-1}. Rician K=5 provides 5-7dB gain over Rayleigh through LOS component. The 100Hz Doppler introduces ICI power proportional to normalized frequency offset squared, becoming dominant for 64-QAM's tight constellation spacing.

E. Result 5: BER vs Doppler

Figure 7 analyzes BER degradation as Doppler frequency increases at fixed SNR.

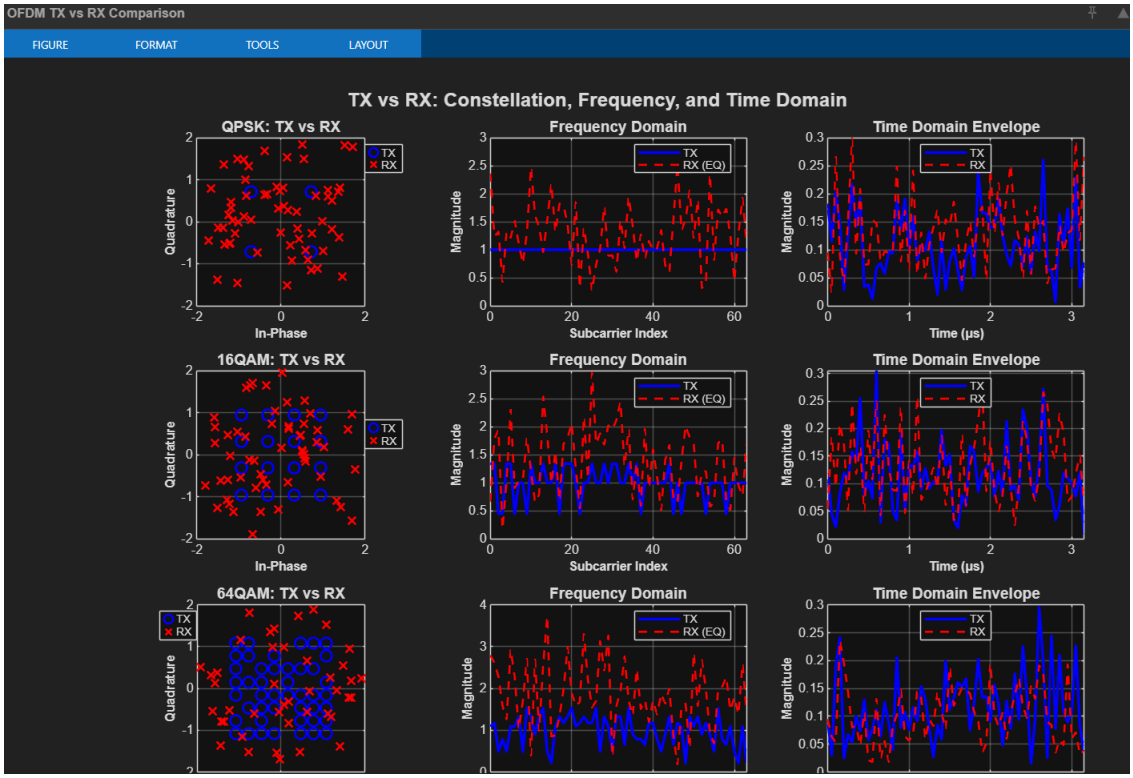

Fig. 5: TX vs RX Comparison across constellation, frequency domain, and time domain for QPSK, 16-QAM, and 64-QAM modulation schemes, illustrating the impact of channel impairments.

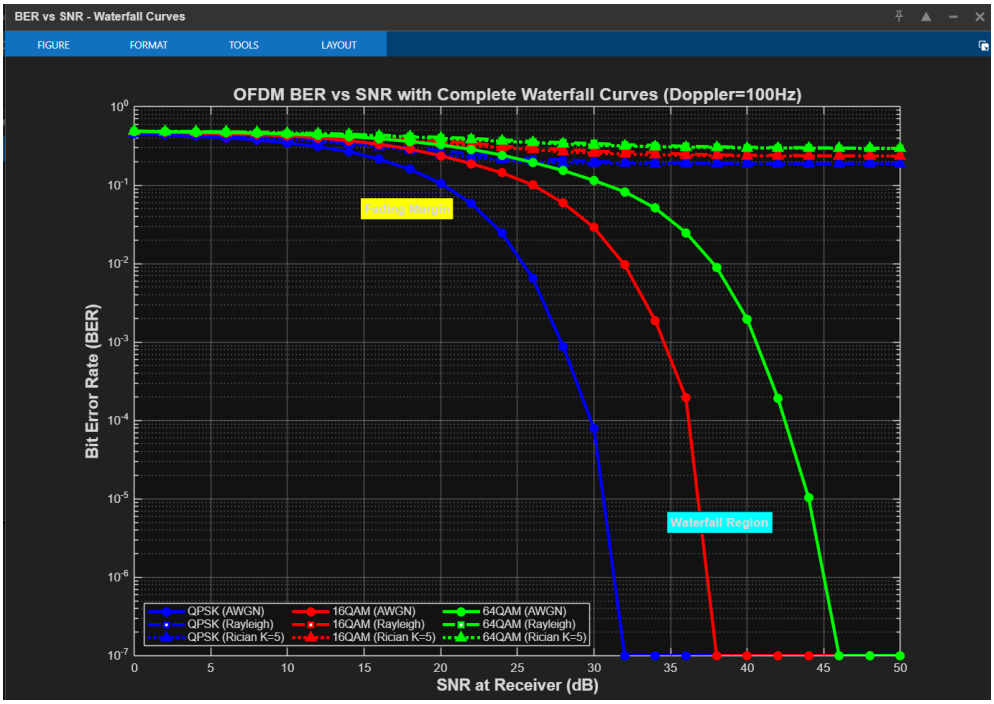

Fig. 6: BER vs SNR waterfall curves with complete comparison for QPSK, 16-QAM, and 64-QAM under AWGN, Rayleigh fading (Doppler=100Hz), and Rician fading (K=5) channels.

Simple Explanation: This plot reveals how mobility affects communication at constant signal strength (20dB). As Doppler increases (representing speeds from 0 to 162 km/h), BER worsens for all modulations. QPSK (blue) stays relatively flat, maintaining acceptable errors even at high speeds. 16-QAM (red) degrades noticeably above 150Hz. 64-QAM (green)

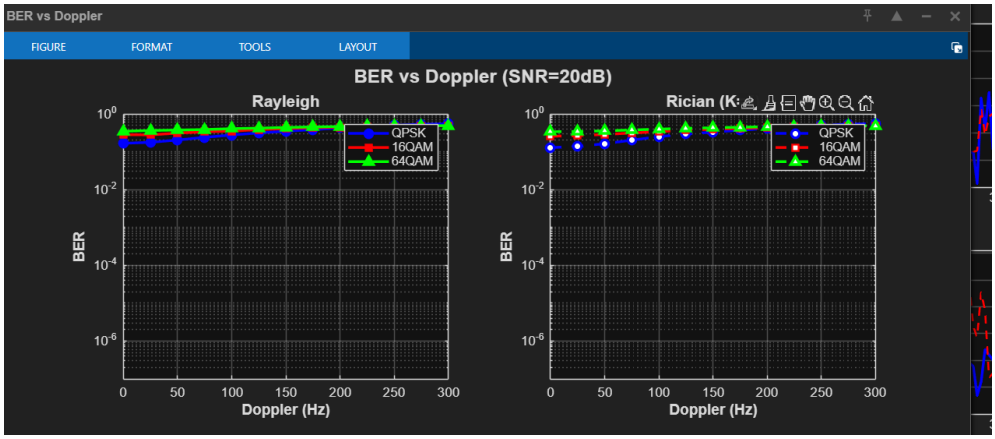

Fig. 7: BER vs Doppler frequency at SNR=20dB for QPSK, 16-QAM, and 64-QAM under Rayleigh and Rician (K=5) fading channels, demonstrating the impact of user mobility.

fails catastrophically beyond 50Hz. Rician channels (right) consistently outperform Rayleigh (left) due to strong line-of-sight component.

Technical Explanation: For Rayleigh fading, QPSK maintains BER below 10^{-1} across entire 0-300Hz range due to large symbol spacing, exhibiting gradual degradation from 5×10^{-2} at 0Hz to 8×10^{-2} at 300Hz. 16-QAM shows inflection at 150Hz where ICI power equals half-symbol spacing energy, causing BER escalation from 10^{-1} to 3×10^{-1}. 64-QAM experiences failure beyond 50Hz with BER saturating at 0.45 as ICI-induced phase rotation exceeds decision boundaries. Rician K=5 provides 10-12dB effective SNR improvement, reducing QPSK BER to 10^{-2} and extending 16-QAM viability to 200Hz.

V. Conclusion

This study comprehensively analyzed the impact of Doppler-induced frequency offset on OFDM system performance across different modulation schemes and fading channels. Results demonstrate that QPSK maintains superior BER performance under high Doppler conditions (up to 300 Hz) in both Rayleigh and Rician channels, making it the preferred choice for high-mobility applications such as vehicular communications. While 16-QAM and 64-QAM offer higher spectral efficiency, they suffer significant performance degradation beyond 50-150 Hz Doppler shift, limiting their applicability in mobile scenarios. The presence of a LOS component in Rician fading provides consistent 3-5 dB performance improvement over Rayleigh fading across all conditions. The waterfall curves reveal that achieving target BER of 10^{-5} under 100 Hz Doppler requires approximately 35 dB SNR for QPSK, 40 dB for 16-QAM, and becomes impractical for 64-QAM, highlighting the fundamental trade-off between spectral efficiency and robustness. These findings suggest that practical OFDM systems should implement adaptive modulation and coding schemes that dynamically adjust modulation order based on estimated Doppler frequency and channel conditions. Future work should investigate advanced ICI cancellation techniques, pilot-aided channel estimation under high mobility, and machine learning-based adaptive schemes to further enhance OFDM performance in time-varying channels.

References

[1] I. R. Capoglu, Y. Li, and A. Swami, "Effect of Doppler spread on OFDM based UWB system," *IEEE 5th Workshop on Signal Processing Advances in Wireless Communications*, Lisbon, Portugal, 2004, pp. 145-149.

[2] H. Zhu, L. Bouchard, and L. Boucher, "Performance of OFDM based wireless LAN system under Doppler over Rayleigh fading," *International Conference on Communication Technology Proceedings (ICCT)*, Beijing, China, 2003, pp. 1234-1237, vol. 2.

VI. For MATLAB code refer to this Github link:

GitHub Repository: *https://github.com/MichaelZachariah/CE2-OFDM-Doppler-impact-code-*